Vibrationally promoted electron emission from low work-function metal surfaces

Jason D. White, Jun Chen,[a] and Daniel Matsiev
Department of Chemistry and Biochemistry, University of California at Santa Barbara, Santa Barbara, California 93106-9510

Daniel J. Auerbach
Hitachi Global Storage Technologies, 650 Harry Road, San Jose, California 95120-6099

Alec M. Wodtke[b]
Department of Chemistry and Biochemistry, University of California at Santa Barbara, Santa Barbara, California 93106-9510

(Received 5 October 2005; accepted 16 December 2005; published online 8 February 2006)

We observe electron emission when vibrationally excited NO molecules with vibrational state **v**, in the range of $9 \leqslant \mathbf{v} \leqslant 18$, are scattered from a Cs-dosed Au surface. The quantum efficiency increases strongly with **v**, increasing up to 10^{-2} electrons per NO (**v**) collision, a value several orders of magnitude larger than that observed in experiments with similar molecules in the ground vibrational state. The electron emission signal, as a function of **v**, has a threshold where the vibrational excitation energy slightly exceeds the surface work function. This threshold behavior strongly suggests that we are observing the direct conversion of NO vibrational energy into electron kinetic energy. Several potential mechanisms for the observed electron emission are explored, including (1) vibrational autodetachment, (2) an Auger-type two-electron process, and (3) vibrationally promoted dissociation. The results of this work provide direct evidence for nonadiabatic energy-transfer events associated with large amplitude vibrational motion at metal surfaces. © *2006 American Institute of Physics*. [DOI: 10.1063/1.2166360]

INTRODUCTION

Developing a fundamental understanding of chemical reactions at metallic surfaces has long been of substantial interest to the surface science community, especially due to its potential relevance to heterogeneous catalysis. Among a host of other topics, *environmental* catalysis has been the focus of much study, with, for example, an eye toward understanding the surface chemistry controlling atmospheric NO_x emissions.[1] NO and NO_2 formed by internal combustion engines are crucially important in the ozone forming chemistry of urban smog. The application of metallic catalysts capable of removing NO_x from combustion emissions has been a major breakthrough which points out the practical importance of this area of surface science.

The deepest level of understanding for elementary chemical reactions has been achieved for cases where high level theoretical methods as well as quantum state resolved experimental measurements have been possible. Most of these examples are gas-phase chemical reactions where "chemically accurate" potential-energy surfaces can be calculated.[2]

The Born-Oppenheimer approximation,[3] (BOA) is central to modeling reaction dynamics in gas-phase reactions. In its simplest form, the BOA assumes that when describing molecular wave functions the electronic and nuclear motions can be separated: indeed, nuclear motion is orders of magnitude slower than that of electrons, and hence, electronic rearrangement occurs instantaneously when compared to the time scales of molecular vibrations. As a result, the reacting system proceeds along the potential-energy surface (PES) associated with its ground electronic state.

The success of this approach in modeling gas-phase reactions has spurred the application of the BOA to molecular interactions at metal surfaces. There are, however, many essential differences between molecule-molecule interactions in the gas phase and those at the molecule-surface interface. In the gas phase, molecules often have widely spaced electronic states and are traveling at relatively slow speeds. At a metal surface, the situation changes dramatically. Above the Fermi Level of the metal, there are many closely spaced, low lying, unoccupied electronic states that can give rise to electronic excitations which violate the assumptions inherent in the BOA. If a reacting molecule incident upon the metal surface can promote electrons to low-energy unoccupied orbitals, a new picture of chemical reactivity involving excited electrons and holes will be required. Some theoretical progress in this direction has been made.[4]

In an recent review, Wodtke *et al.*[5] discuss the importance of understanding violations of the BOA and give specific examples of where the BOA is applied incorrectly. They cite the Massey criterion,[6]

[a]Present address: Department of Chemistry and Chemical Biology, Cornell University, Ithaca, NY 14853-1301.
[b]Author to whom correspondence should be addressed. Electronic mail: wodtke@chem.ucsb.edu

$$\frac{\hbar\mu\dot{\mathbf{R}}\cdot\mathbf{d}_{12}}{|\mathcal{E}_1-\mathcal{E}_2|}\ll 1, \tag{1}$$

as a good tool for predicting adiabatic behavior. Here, μ is the reduced mass, $\dot{\mathbf{R}}$ is the nuclear velocity, $\mathbf{d}_{12}$ is the nonadiabatic coupling, and $\mathcal{E}_1-\mathcal{E}_2$ is the separation in energy between the two electronic states. In gas-phase interactions, the energy gaps between levels are often large, which ensures that Eq. (1) is true. When the separation in energy is small, as is the case for the electronic states of metals, the Massey criterion may no longer be valid.

Systems such as CO on Ru(0001),[7] O_2 on Mg (0001),[8] and H_2 on Cu (Ref. 9) are good examples where dynamics appear to be well explained using the assumptions inherent to the BOA. There is, however, growing evidence that for some systems, theories that go beyond the BOA are needed for a full understanding.

The possible importance of nonadiabatic effects in vibrational energy transfer at surfaces was suggested over 20 years ago by Rettner *et al.* in studies of the vibrational excitation of NO scattering from a Ag(111) surface.[10] The energy and surface temperature dependence of the excitation process strongly suggested a process involving the decay of thermally excited electron-hole pairs (EHP) in the collision process. More detailed theoretical work by Gadzuk and Holloway[11] and Newns[12] implicated a mechanism for vibrational excitation of the NO molecules by EHP energy exchange, a mechanism that violates the BOA.

The conclusions of that work were later called into question[13] when it was shown that an adiabatic mechanism might be capable of explaining the observed vibrational excitation. Gross and Brenig[14] modified the Newns-Anderson model[12] to investigate the problem of adiabatic versus nonadiabatic energy transfer. With different potential parameters, they were able to construct an adiabatic theory that agreed with experimental observations, in particular, the increase of the vibrational excitation probability as a function of increasing translational energy. They then calculated the vibrational survival probability of NO ($\mathbf{v}=1$) as a function of kinetic energy. Under the adiabatic mechanism, it was predicted that the survival probability would remain near unity at all translational energies, but would drop rapidly to zero at energies larger than 0.7 eV if nonadiabatic transfer was important. In 2000, Huang *et al.*,[15] measured the survival probability dependence on incidence energy when scattering NO ($\mathbf{v}=2$) from a Au(111) surface. They observed a decrease in survival probability with increasing incidence energy, a result in qualitative agreement with Gross and Brenig's predictions for an electronically nonadiabatic mechanism.

In more recent work, highly vibrationally excited NO molecules were scattered from a metal surface.[16] Inelastic scattering of NO ($\mathbf{v}=15$) from Au(111) showed efficient loss of as many as ten vibrational quanta, whereas similar experiments carried out on lithium fluoride (LiF) showed little vibrational energy transfer.[17] To explain these results, an electronically nonadiabatic mechanism involving electron transfer accompanied by vibrational deexcitation was suggested. Here, for Au(111), a metal electron hops to the molecule when the bond is stretched at the outer turning point of vibration, and then transfers back to the metal as the molecule's bond compresses. In the case of LiF, the large band gap of the insulator suppresses electron transfer and effectively turns off this electronic mechanism for vibrational relaxation. Later theoretical work employing a similar mechanism,[18] reproduced the measurements of vibrational relaxation on Au(111) reasonably well.

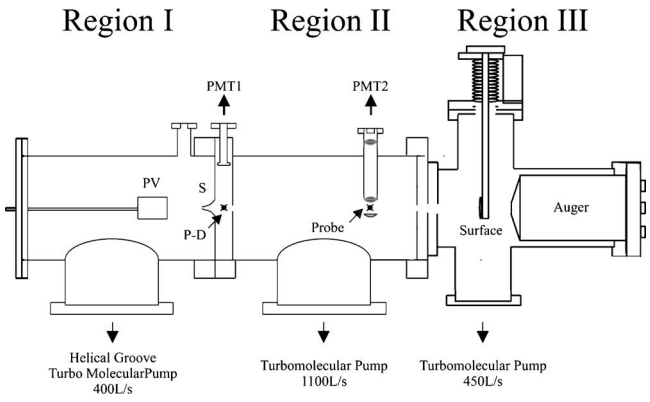

FIG. 1. Schematic diagram of the apparatus. The supersonic NO beam expands from the pulsed valve (PV) into a region of high vacuum (10^{-4} Torr) and is collimated by an electroformed skimmer (S). Two-laser optical pumping (P-D) is performed after the skimmer and the fluorescence emission and fluorescence depletion are collected with a photomultiplier tube (PMT1). The prepared molecules travel downstream through region II, where optical probing is carried out using PMT2. The third and final chamber is an UHV (10^{-10} Torr) chamber where the low work-function Cs/Au surfaces are prepared. Region III is also where scattering occurs and electron emission is detected.

These results on vibrational energy transfer seemed to indicate indirectly that nonadiabatic processes were occurring during charge transfer when molecules collided with the surface. Direct observation of these processes should spark interest in the development of models which fully incorporate nonadiabatic energy transfer.

In a short Letter,[19] we recently reported the direct observation of electron emission from metallic surfaces. In particular, highly vibrationally excited NO molecules were scattered from low work-function (1.3–1.6 eV) (Ref. 20) Cs/Au surfaces and the electron emission was measured as a function of the vibrational energy of the incoming NO molecules. In that work, we observed both a clear threshold for electron emission near the surface work function and a maximum quantum yield approaching 10^{-2}. Both of these features are important when developing the mechanism for this process. The current work presents a more comprehensive exposition of our work and analysis of our data, with an emphasis on possible underlying mechanisms for this process.

EXPERIMENT

A schematic representation of our apparatus is shown in Fig. 1. It consisted of three differentially pumped chambers, all evacuated by turbo-molecular pumps: a source chamber (region I, 10^{-4} Torr during operation), a probe chamber (region II, 10^{-8} Torr), and an UHV surface chamber (region III, 5×10^{-10} Torr). The source chamber utilized a pulsed supersonic expansion of NO molecules. Optical pumping tech-

niques for efficient state preparation and probing were used in region II. Region III housed surface science equipment where low work-function surfaces were prepared and the scattering experiments were carried out.

Region I: Source

A pulsed (10 Hz repetition rate) piezoelectric valve (PV) with a 1 mm opening was used to create a supersonic beam of molecular NO (15% seeded in Kr at a stagnation pressure of 3 atm) with rotational temperature of 4 K and kinetic energy of 29 meV (0.67 kcal/mol). The beam was collimated by a 2 mm electroformed skimmer (S-Beam Dynamics, Inc.) placed 3 cm from the nozzle prior to passing into region II.

Region II: Optical preparation and detection

Region II was equipped with the capability to prepare NO molecules in high vibrational states using stimulated emission pumping[21] (SEP),[22] a two-laser technique that transfers population of NO from $\mathbf{v}''=0$ into the excited vibrational state through an intermediate electronic state or Franck-Condon pumping (FCP).[23] The stimulated emission step in SEP was monitored with fluorescence depletion spectroscopy using a photomultiplier (PMT1-Hamamatsu R212UH), and the highly vibrationally excited molecules were detected downstream using laser-induced fluorescence (LIF) at the point marked probe with a second photomultiplier tube (PMT2-Hamamatsu R7154).

Stimulated emission pumping

The electronic landscape for preparation of NO in various vibrational states is the same as shown by Chen *et al.*[24] Here, we describe the procedure to prepare $\mathbf{v}''=18$ using SEP, but the method was similar for $4 \leqslant \mathbf{v} \leqslant 18$. The pump laser excited NO molecules via the $A\,^2\Sigma^+(\mathbf{v}=3) \leftarrow X\,^2\Pi_{1/2}(\mathbf{v}=0)$ transition at ~195.5 nm, where the light was generated by sum-frequency mixing in the following manner. A seeded Nd:YAG (yttrium aluminum garnet) laser (Spectra Physics LAB-170) simultaneously produced 150 mJ/pulse at 532 nm and 100 mJ/pulse at 266 nm. A dye laser (Sirah CSTR-DA-24) operating on LDS 751 was pumped with the 532 nm light. The tunable output of the dye (~737 nm) and the 266 nm light were sum-frequency mixed using a beta barium borate (BBO) crystal to yield the pump pulse near 195 nm with energy of 1 mJ/pulse.

The dump laser, at approximately 460 nm, stimulated emission into the $\mathbf{v}''=18$ level of the ground electronic state, $A\,^2\Sigma^+(\mathbf{v}=3) \rightarrow X\,^2\Pi(\mathbf{v}=18)$. For this band, the third harmonic of a Nd:YAG laser (Spectra Physics PRO-200) pumped a dye laser (Sirah PRSC-DA-24) operating on Coumarin 460, which generated 60 mJ/pulse in the 460–465 nm region.

Franck-Condon pumping

Franck-Condon Pumping (FCP) is a complementary excitation scheme that utilizes spontaneous emission from $\mathbf{v}'$ into $\mathbf{v}''$. Although FCP allows more limited control over the vibrational distribution, it can still be quite useful because significantly different vibrational distributions can be produced by exciting to different $\mathbf{v}'$ vibrational levels. Figure 2 shows two calculated vibrational distributions for spontaneous emission from the $A\,^2\Sigma^+(\mathbf{v}=0)$ and $A\,^2\Sigma^+(\mathbf{v}=3)$ states. These intensities were calculated as $\nu^3_{\mathbf{v}',\mathbf{v}''}\mathbf{q}_{\mathbf{v}',\mathbf{v}''}$, where $\nu_{\mathbf{v}',\mathbf{v}''}$ is the frequency of the transition and $\mathbf{q}_{\mathbf{v}',\mathbf{v}''}$ is the Franck-Condon factor between the two vibrational states. The wide gray bars refer to the final vibrational distribution produced in $\mathbf{v}''$ after pumping the $A\,^2\Sigma^+(\mathbf{v}=3) \leftarrow X\,^2\Pi_{1/2}(\mathbf{v}=0) \times [A\text{-}X\ 3\text{-}0]$ transition. Similarly, the black narrow bars refer to $A\,^2\Sigma^+(\mathbf{v}=0) \leftarrow X\,^2\Pi_{1/2}(\mathbf{v}=0)[A\text{-}X\ 0\text{-}0]$ excitation. Because the work function of the surface is 1.3–1.6 eV, it is clear that *A-X* 3-0 efficiently prepares molecules with vibrational energy larger than the work function, while *A-X* 0-0 does not. The importance of this difference will be presented later.

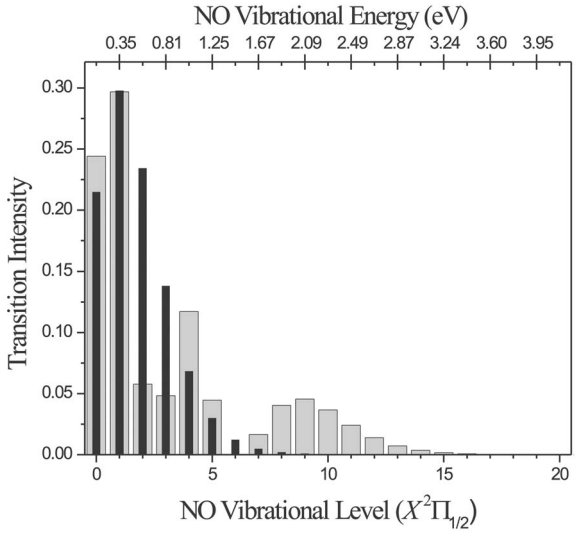

FIG. 2. Vibrational state population produced by two Franck-Condon pumping schemes. Population distributions produced by spontaneous emission from two vibrational levels of the excited electronic $A\,^2\Sigma^+$ state of NO. (*A-X* 3-0, gray bars), intensities from pumping $A\,^2\Sigma^+(\mathbf{v}=3) \leftarrow X\,^2\Pi_{1/2}(\mathbf{v}=0)$ and (*A-X* 0-0, black bars), intensities from pumping $A\,^2\Sigma^+(\mathbf{v}=0) \leftarrow X\,^2\Pi_{1/2}(\mathbf{v}=0)$.

Probing the molecular beam

The prepared vibrational state population was probed 50 cm from the nozzle (Probe in Fig. 1) employing the $B\,^2\Pi(\mathbf{v}=1) \leftarrow X\,^2\Pi_{1/2}(\mathbf{v}=18)$ band for LIF with a third Nd:YAG pumped dye laser operating at approximately 582.4 nm. This light was produced by a Continuum ND6000 dye laser running a mixture of Rhodamine 590 and Rhodamine 610 pumped by the second harmonic of a Continuum Nd:YAG (Model 7010), which allowed generation of ~20 mJ/pulse: enough to saturate the probe transition.

Fluorescence was collected and measured with a solar-blind photomultiplier tube (PMT2) that efficiently suppressed the scattered light background. The wavelength-dependent response of PMT2 could be tested directly by comparing signal intensities from equal numbers of molecules prepared by the probe laser in $B\,^2\Pi$ $(\mathbf{v}=1)$ and $B\,^2\Pi$ $(\mathbf{v}=2)$, which exhibit different fluorescence spectra.

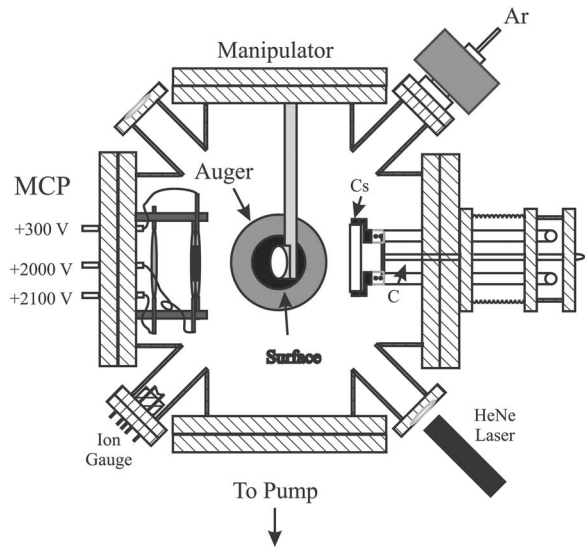

FIG. 3. Head-on view of the UHV surface chamber. The surface chamber is equipped with a SAES Getters cesium (Cs) doser, a HeNe laser for photoemission, a metal collector biased at +50 V (C) for collection of photoelectrons during deposition, a multichannel plate (MCP) assembly for electron emission experiments, an Ar (Ar) bombardment gun for sputtering, and an Auger spectrometer for surface cleanliness measurements. Other details can be found in the text.

Based on specifications of the solar-blind PMT and theoretically calculated emission spectra for $B\,^2\Pi$ ($\mathbf{v}=1$ and 2), the predicted fluorescence ratio for $B\,^2\Pi$ ($\mathbf{v}=1$) and $B\,^2\Pi$ ($\mathbf{v}=2$) compared well with the observed ratio. This allowed us to conclude that the wavelength-dependent response of the solar-blind PMT results in a 33% detection efficiency for the fluorescence photons produced from the $B\,^2\Pi$ ($\mathbf{v}=1$) state used in the probe step.[25]

Region III: Detection of electron emission

A 1 mm aperture separated region II from region III (the surface scattering chamber) to preserve differential pumping and maintain region III at 10^{-10} Torr. A view of region III from the perspective of the molecular beam can be seen in Fig. 3. The chamber contains a 1.18 cm gold crystal[26] surface mounted on a manipulator with translational and rotational motions. A substrate heater (Heatwave Labs-"Button Heater" Model No. 101137) was used to heat the surface while baking the chamber. The gold surface was cleaned by cycles of sputtering with an Ar^+-ion gun (Ar) and charactered by Auger electron spectroscopy (Phi Electronics) until low contaminant levels (primarily carbon) were achieved. The low work-function surfaces were prepared by depositing submonolayer amounts of cesium onto gold using a commercially available cesium chromate doser (Cs-SAES Getters Model Cs/NF/3.9/12 FT10+10). To insure reproducibility, a helium-neon laser (HeNe laser) was used to induce photoemission during cesium deposition, and the photoelectrons were collected with a metal collector (C). Cesium coverage was stopped at the time of maximum photoemission, which is assumed to be approximately the surface work-function minimum.[27]

After dosing, the surface was promptly rotated into position for the scattering experiment. Electrons were detected by a double-microchannel plate (MCP) detector in a chevron configuration placed 5 cm from the surface. The front of the detector was biased at +300 V to improve electron collection efficiency and to exclude any potential signals from positively charged particles. By increasing the positive voltage (shown in Fig. 3 as 2000 and 2100 V) the gain of the MCP could be varied up to 10^6–10^7.[28]

We observed a strong dependence for particle detection on MCP active area and magnetic fields which provided evidence that the particles were electrons.[29] With a permanent magnet of 2–3 G, we were able to completely suppress the signal from the scattering event. If the particles were electrons, a magnetic field of this strength in our system should extinguish the signal, whereas for negatively charged molecules, the signal would remain. The output of the MCP was processed by either an oscilloscope (LeCroy WaveRunner LT344) for laser scanning experiments or a multichannel scaler (EG&G Ortec 914 TurboMCS) operating as a counter to measure electron emission events and for time-of-flight (TOF) measurements.

Determination of the absolute quantum yield

In order to calculate the quantum yield for vibrationally promoted electron emission, it is essential to know the absolute number of electrons generated in the scattering event and the absolute number of vibrationally excited molecules (N_v) incident on the surface.

The number of electrons was measured by summing the electron counts recorded by the multichannel scaler (MCS) during the experiment. The MCS discriminator was set such that a small signal from random events ($<5\%$ peak signal for $\mathbf{v}''=18$) was observed to ensure that each electron from the NO scattering event that strikes the MCP was counted with near unit efficiency, as determined from a signal saturation as a function of MCP voltage measurement. This background signal was subtracted from the total signal when determining the number of electrons detected during scattering. The assumption that we collect every electron at the MCP yields a lower limit to the true quantum efficiency, so if the collection efficiency was less than unity, the quantum efficiencies reported here would need to be increased.

To measure the number of vibrationally excited molecules at the surface, we installed the LIF detection system (marked PMT2 in Fig. 1) at the position of the surface in region III. We then used the tunable probe laser to induce fluorescence from the beam of NO ($\mathbf{v}''=18$) prepared by SEP, from which the incident molecular-beam intensity, N_{18}, could be derived.

The results of this measurement showed that the number of NO ($\mathbf{v}''=18$) molecules incident on the surface in each pulse was $\sim 3\times 10^4$ (Ref. 30) The same LIF collection assembly was then moved to probe the point in region II marked probe in Fig. 1, where accordingly larger fluorescence intensity was observed. The observed ratio of signals between regions II and III compared favorably with a geometrical estimate. This region II probe signal could then be used to calibrate the flux of vibrationally excited molecules incident on the surface periodically during further measurements.

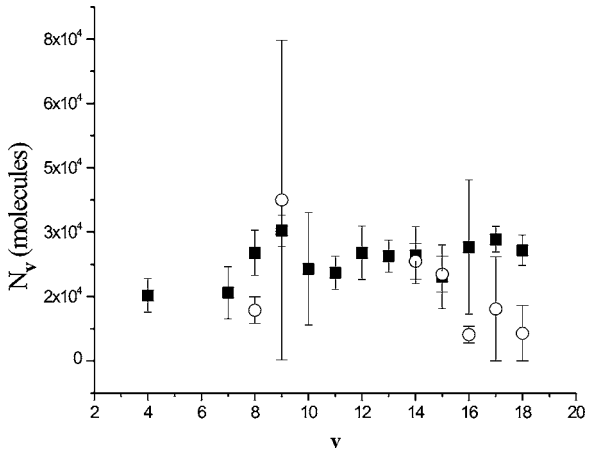

FIG. 4. Determination of the number of vibrationally excited molecules. The number of molecules was determined by probing the vibrationally excited molecules along the $B\,^2\Pi(\mathbf{v}=1)\leftarrow X\,^2\Pi_{1/2}(\mathbf{v})$ band and evaluating as described in the text. This result is shown by the open circles. Fluorescence depletion measurements (solid squares) are also shown. Agreement is good and does not vary by more than a factor of 3. Here, error bars are constructed from 99.99% confidence limits to insure the greatest percentage of molecules is accounted for.

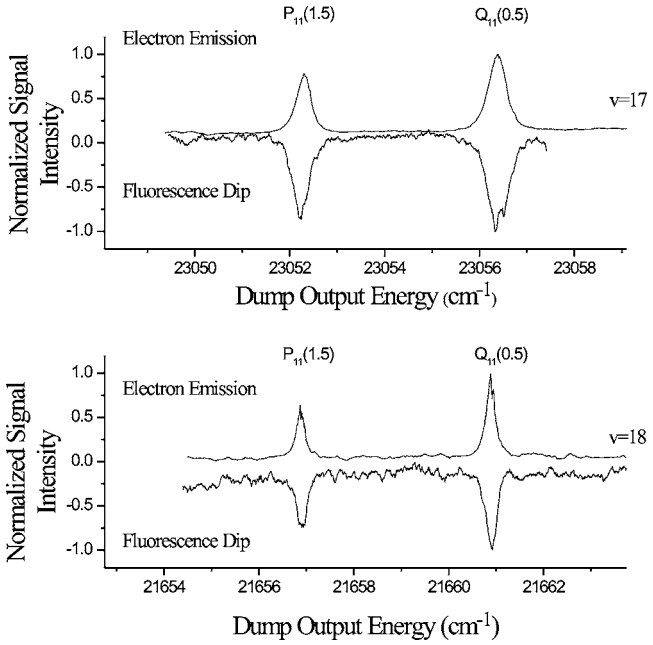

FIG. 5. Spectral scans for various dump transitions. Electron emission from scattering of NO ($\mathbf{v}''=17$ and 18) off Cs/Au surface (upward peaks) is shown along with corresponding transitions populating high vibrational levels of $X\,^2\Pi$ state of NO (downward peaks) as a function of dump laser photon energy. The peak-to-peak separation for $Q_{11}(0.5)$ to $P_{11}(1.5)$ is consistent with the energy separation for these rotational bands for these vibrational states.

Small Franck-Condon Factors as well as some technical problems with the laser setup prevented us from using the region II probe signal for every vibrational state. So, it was necessary to find alternate means to quantify the number of molecules. To do this, we assumed that the number of vibrationally excited molecules is linearly dependent on the fluorescence depletion signal and linearly proportional to the pump laser-induced fluorescence, which was nearly constant from day to day. This approach relied exclusively on the fractional depletion induced by the laser and the pump-step LIF signal measured on PMT1 of Fig. 1.

For this calibration, two bands, $B\,^2\Pi(\mathbf{v}=1)\leftarrow X\,^2\Pi_{1/2}(\mathbf{v}=14)$ and $B\,^2\Pi(\mathbf{v}=1)\leftarrow X\,^2\Pi_{1/2}(\mathbf{v}=15)$ which showed saturation of the probe signal as confirmed by a laser power dependence measurement, were used to measure the number of molecules detected with the probe laser as a function of the fluorescence depletion. Here, we used the Sirah laser for probing as it had a more defined laser spot than the Continuum laser, which was used for measuring the transmission efficiency between region II and region III. Figure 4 compares the number of molecules in each vibrational state obtained by two methods: (1) detected with the probe laser (open circles) and (2) determined by the fluorescence depletion calibration (black squares). The two methods agree reasonably well for all cases where direct comparison can be made. The error bars reflect systematic uncertainties inherent in laser excitation of the molecular beam. The growing discrepancy between $\mathbf{v}''=14$ and 18 is believed to be due to the increasing difficulty in achieving saturation of the probe LIF transition with increasing $\mathbf{v}$. The relatively large systematic discrepancy exhibited by the comparison between the fluorescence depletion and probe measurements is the major source of the reported error bars for the quantum yield measurement, which will be discussed below.

RESULTS

SEP observed by electron emission

We can unambiguously verify that the scattering of vibrationally excited NO molecules from the Cs/Au surface is the direct cause of the observed electron emission simply by monitoring the fluorescence depletion and electron emission signals during a fluorescence depletion laser scan, as shown in Fig. 5. One can clearly see that electron emission signal (upward peaks) exhibits a one-to-one correspondence with the fluorescence depletion (downward peaks), thus confirming that the electron emission from the low work-function surface occurs only when highly vibrationally excited NO is produced.

Observed fluorescence depletion transitions frequencies were compared to the theoretical values calculated according to Herzberg[31] and are shown in Table I. Close inspection shows that the theoretical calculation varies by 30 to 200 cm^{-1} from the experimentally determined transition energy. This is attributed to errors in absolute wavelength calibration of the various lasers. To ensure certainty in the spectroscopic analysis, we also report combination differences $\Delta'(0.5)$, which are the frequency differences between the measured $Q_{11}(0.5)$ and $P_{11}(1.5)$ dump transitions. Realizing that these two transitions share a common upper state, we recognize that the combination differences are energy gaps between rotational levels of the vibrationally excited ground electronic state. The comparison between theory and experiment for the combination differences is also shown in Table I and is generally within 0.1 cm^{-1}. The transition labels used

TABLE I. Dump transitions were generated via frequency doubling the dye fundamental with the exception of $v=17$ and $v=18$. Transitions $\mathbf{v}=10$ to $\mathbf{v}=16$ were prepared using Continuum laser as dump.

	Dump laser $Q_{11}(0.5)$		Dump laser $P_{11}(1.5)$		$\Delta'(0.5)=Q_{11}(0.5)-P_{11}(1.5)$		Agreement
Transition	Theory (cm^{-1})	Experiment (cm^{-1})	Theory (cm^{-1})	Experiment (cm^{-1})	Theory (T) (cm^{-1})	Experiment (E) (cm^{-1})	T-E (cm^{-1})
$A(3)\rightarrow X(7)$	38 658.45	38 594.09	38 653.82	38 589.33	4.63	4.77	−0.13
$A(3)\rightarrow X(8)$	36 978.14	36 914.22	36 973.57	36 909.32	4.58	4.90	−0.33
$A(3)\rightarrow X(9)$	35 325.59	35 262.47	35 321.07	35 257.06	4.53	5.41	−0.88
$A(3)\rightarrow X(10)$	33 700.76	33 882.80	33 696.28	33 878.21	4.48	4.59	−0.11
$A(3)\rightarrow X(11)$	32 103.58	32 273.47	32 099.16	32 269.10	4.43	4.37	0.05
$A(3)\rightarrow X(12)$	30 534.03	30 665.72	30 529.65	30 661.21	4.37	4.51	−0.14
$A(3)\rightarrow X(13)$	28 992.04	29 196.44	28 987.72	29 192.00	4.32	4.44	−0.12
$A(3)\rightarrow X(14)$	27 477.59	27 627.21	27 473.31	27 622.94	4.27	4.27	0.00
$A(3)\rightarrow X(15)$	25 990.61	26 125.49	25 986.39	26 121.25	4.22	4.23	−0.01
$A(3)\rightarrow X(16)$	24 531.07	24 653.25	24 526.90	24 649.06	4.17	4.19	−0.02
$A(3)\rightarrow X(17)$	23 098.91	23 056.40	23 094.79	23 052.26	4.12	4.15	−0.03
$A(3)\rightarrow X(18)$	21 694.10	21 660.92	21 690.03	21 656.88	4.07	4.03	0.03

follow the convention described in White *et al.*[32] In the remainder of this work, only $Q_{11}(0.5)$ transition were used to prepare vibrationally excited NO molecules.

Franck-Condon pumping

While a detailed measurement of the vibrational dependence of electron emission can be obtained using SEP (see below), FCP is a convenient way to obtain a coarse picture of the characteristics of the experiment. When using the pump laser alone to excite NO through the $A\,^2\Sigma^+(\mathbf{v}=3)\leftarrow X\,^2\Pi_{1/2}(\mathbf{v}=0)$ band at the position marked P-D in Fig. 1, electron emission was induced 65 cm downstream at the surface 1.43 ms after the laser was fired. The following evidence indicates that the long-lived vibrationally excited molecules are interacting with the surface and creating this signal. The fluorescence lifetime of the $A\,^2\Sigma^+$ state is around 200 ns (Ref. 33) which, through spontaneous emission, prepares the NO molecules in $X\,^2\Pi$ with the vibrational distribution shown as wide gray boxes in Fig. 2. The radiative lifetimes for these vibrationally excited states are longer than the time of flight for the excited packet. For example, the radiative lifetime for NO $\mathbf{v}''=18$ is 3 ms,[34] roughly double the flight time to the surface (1.43 ms).

Figure 6 shows TOF electron emission signal obtained in this way. Using the flight distance and the arrival time, one may derive the molecular beam's most probable speed, 455 m/s. The full width at half maximum (FWHM) of the speed distribution is 37 m/s, which is consistent with what is expected for a supersonic expansion ($\Delta v/v\sim 10\%$). The probe laser may also be used to determine the velocity of the molecular beam by adjusting the Q-switch firing time with respect to the laser. Hence, the maximum in fluorescence over the beam pulse corresponds to the most probable velocity of the molecular beam, 457 m/s, which is nearly equal to the velocity obtained from the TOF electron emission measurement.

The root-mean-square (rms) speed of the molecular beam can be predicted for our NO/Kr mixture using the simple formula,

$$v_{\mathrm{rms}}=\sqrt{\frac{2\bar{C}_pT}{\bar{m}}}, \tag{2}$$

where $\bar{C}_p$ is the average heat capacity at constant pressure (45 J K^{-1} mol^{-1}) and $\bar{m}$ is the average mass (75.73 amu). Using Eq. (2), we arrive at a v_{rms} of 422 m/s. This is 7% smaller than the measured speed (455 and 457 m/s), likely the result of imperfections in our gas mixing procedures. From this analysis and the previous results, it is clear that the long-lived vibrationally excited molecules produced by FCP or SEP are responsible for the electron emission.

We may gain approximate information about the vibrational energy required to induce electron emission by chang-

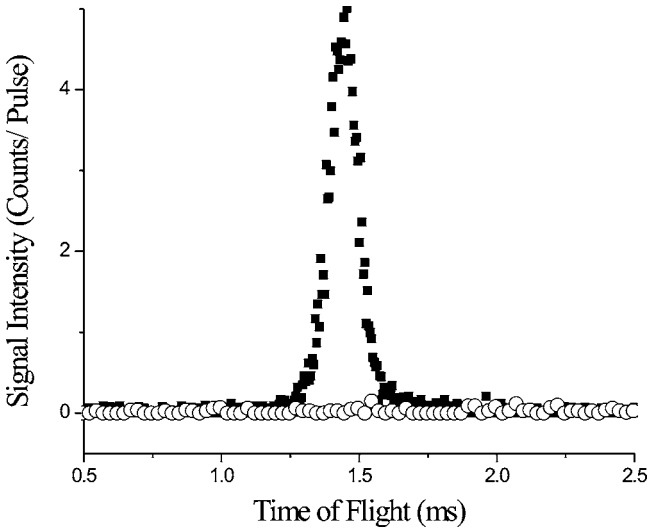

FIG. 6. Arrival time of NO molecules generating electron emission. Here electron emission is generated by NO molecules prepared with the pump laser. The data come in the form of time-of-flight measurements and are similar for SEP experiments. Franck-Condon pumping via the $A\,^2\Sigma^+(\mathbf{v}=3)\leftarrow X\,^2\Pi_{1/2}(\mathbf{v}=0)$ band (solid squares) yields electron emission but FCP via the $A\,^2\Sigma^+(\mathbf{v}=0)\leftarrow X\,^2\Pi_{1/2}(\mathbf{v}=0)$ (open circles) gives no detectable electron emission signal. We attribute this to the population available in vibrational levels larger than the work function of the surface when using the $A\,^2\Sigma^+(\mathbf{v}=3)\leftarrow X\,^2\Pi_{1/2}(\mathbf{v}=0)$ band (see text and Fig. 2).

ing the wavelength of the laser used in FCP so that one excites NO in the $A\,^2\Sigma^+\,(\mathbf{v}=0) \leftarrow X\,^2\Pi\,(\mathbf{v}=0)$. This is shown as open circles in Fig. 6. Despite our best attempts, no discernable electron emission was observed. This negative result is attributed to the differences between the vibrational distributions produced in the two FCP experiments (see Fig. 2). Specifically, the $A\,^2\Sigma^+\,(\mathbf{v}=3) \leftarrow X\,^2\Pi\,(\mathbf{v}=0)$ Franck-Condon pattern is capable of producing substantial population in vibrational states $\mathbf{v}$=7-13: states whose vibrational energy exceeds the work function of the surface. This important point, that the vibrational energy must exceed the surface work function to induce electron emission, will appear again in the presentation of the SEP results below.

Another point is important to note in order to understand how the SEP experiments were carried out. During SEP electron emission experiments, blocking the dump laser allows us to routinely monitor the electron emission signal produced by FCP $A\,^2\Sigma^+\,(\mathbf{v}=3) \leftarrow X\,^2\Pi\,(\mathbf{v}=0)$. This, in combination with monitoring the pump-step LIF signal as well as the magnitude of fluorescence depletion, provided an internal standard of the molecular-beam intensity and the electron detection efficiency and thus was an important means of control over day-to-day variations in several key aspects of the experiment.

SEP results: Vibrational dependence of electron emission

The coarse-grain vibrational dependence presented in the FCP experiments with NO motivated us to carry out a full study of the vibrational dependence of the electron emission using SEP. Specific states of NO ($\mathbf{v}''$=4, 7-18) were prepared and scattered from the low work-function surface. The resulting electron emission signal was acquired by a multichannel scaler, and generated TOF distributions for the molecular beam, similar to those seen in Fig. 6. The quantum yields for the scattering events were calculated by dividing the total number of electrons counted over the $\sim$100 μs pulse of the molecular beam by the number of vibrationally excited molecules at the position of the surface obtained by calibration of the probe signal as described above.

A nonzero background from FCP was observed as a consequence of using the *A*-*X* 3-0 transition as the pump step in SEP. To subtract the background contribution, a sequence of steps was carried out as follows. First, the laser prepared vibrationally excited molecules by SEP and the resulting electron emission signal was measured. The dump laser was then mechanically blocked and the FCP-induced signal was collected. The dump laser was unblocked and allowed to again interact with the molecular beam and the emission measured. This procedure was repeated approximately 20 times for each vibrational state.

To calculate the amount of electron emission from vibrationally excited molecules, the FCP signal was subtracted from the total signal as follows:

$$\boldsymbol{\sigma}_{\text{two-laser}} - \boldsymbol{\sigma}_{\text{one-laser}} = \boldsymbol{\sigma}_{\text{apparent}}. \tag{3}$$

Here, $\boldsymbol{\sigma}_{\text{two-laser}}$ is the total signal measured in the SEP counting experiment, $\boldsymbol{\sigma}_{\text{one-laser}}$ is the background signal when the dump was blocked, and $\boldsymbol{\sigma}_{\text{apparent}}$ is the apparent electron emission from vibrationally excited molecules. It is important to note that $\boldsymbol{\sigma}_{\text{one-laser}}$ is not simply the FCP background present during the SEP experiment. When utilizing SEP, the FCP signal will be somewhat reduced because of depopulation of the excited electronic state due to the dump laser. The actual FCP background present during the SEP experiment, $\boldsymbol{\sigma}_{\text{FCP}}$, can be derived using the measured fluorescence depletion signal according to Eq. (4).

$$\boldsymbol{\sigma}_{\text{FCP}} = (1 - \text{FD})\boldsymbol{\sigma}_{\text{one-laser}}. \tag{4}$$

Here, FD is the measured fluorescence depletion when the dump laser interacts with the molecular beam. Finally, combining these two ideas, one can derive the actual SEP-induced electron emission signal produced by the highly vibrationally excited molecules, $\boldsymbol{\sigma}_{\text{SEP}}$.

$$\boldsymbol{\sigma}_{\text{SEP}} = \boldsymbol{\sigma}_{\text{two-laser}} - \boldsymbol{\sigma}_{\text{FCP}} = \boldsymbol{\sigma}_{\text{two-laser}} - (1 - \text{FD})\boldsymbol{\sigma}_{\text{one-laser}}. \tag{5}$$

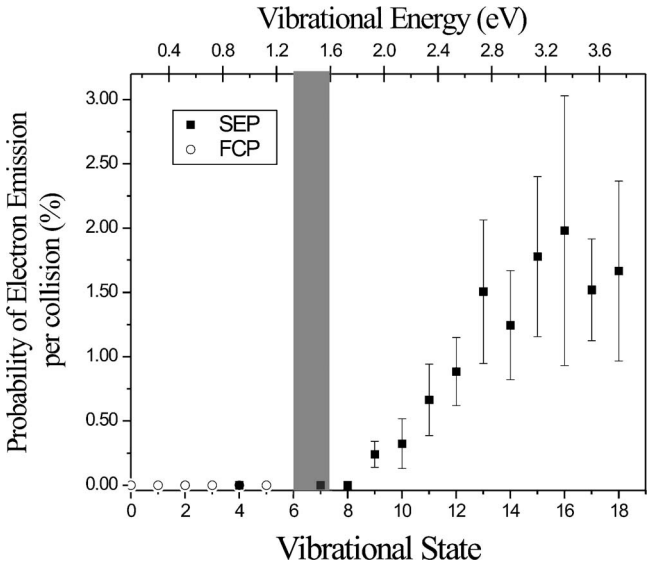

FIG. 7. Plot of electron emission probability as a function of vibrational state and the corresponding vibrational energy. Here the molecules are prepared in one of two ways. The Solid boxes show NO prepared with two-laser SEP technique and the open circles are prepared via FCP *A*-*X* 0-0 (no electron emission possible according to Fig. 2 and 6). It is apparent that there is a vibrational energy threshold for electron emission slightly above the estimated work function of the surface (1.3–1.6 eV, shown as a gray bar). Electron emission probability is determined from the ratio of the number of electrons as determined by electron counting and the vibrationally excited molecule flux at the surface shown as the solid squares in Fig. 4.

The quantum yields for vibrational states measured using SEP are shown in Fig. 7 as closed symbols. The surface work function is also shown as a shaded bar. The open circles are from the observation that the *A*-*X* 0-0 FCP, which populates $\mathbf{v}''$ to $\mathbf{v}$=6, produces no detectible electron emission signal, as shown in Fig. 6. The solid squares of Fig. 7 are derived from the analysis of SEP results described above, utilizing the FCP-normalized beam intensities (solid squares of Fig. 4). The large error bars of Fig. 7 are due principally to the difficulty in accurately determining the absolute number density of the vibrationally excited sample as described above.

Figure 7 reveals two results crucially important to the interpretation of these experiments: (1) the observation of a threshold to vibrationally promoted electron emission approximately coincident yet slightly higher than the surface work function and (2) a maximum 10^{-2} quantum efficiency for vibrationally promoted electron emission. The mechanistic implications of these two observations represent the focus of the following discussion.

DISCUSSION

Much work in the field of chemically induced electron emission from metals invokes an Auger deexcitation process to explain the negative particle emission when (usually) thermal molecules are allowed to interact with low work-function surfaces.[35] It has been successful in describing many gas-surface interactions including O_2, NO, N_2O, and NO_2 on Cs-covered Ru(0001) surfaces. It is with this mechanism that we will begin our discussion.

The Auger deexcitation model, first applied to exoemission during exposure of O_2 on Cs (Ref. 36) by Böttcher *et al.* and further expanded upon by Greber,[37] is summarized as follows. As a molecule approaches a metal surface, the molecule's electron affinity level, e_a, is lowered due to image force interactions. At some distance z (the molecule-surface separation), e_a will plunge below the Fermi level of the surface. In the adiabatic picture for charge transfer, which keeps the system in the lowest-energy configuration at all molecule-surface distances, an electron will transfer from the Fermi level to the molecule at the instant its affinity level crosses the Fermi Level. This is the mechanism commonly known as "harpooning" which was originally developed for gas-phase reactions but has also since been applied to gas-surface reactions by Gadzuk and Noerskov.[38]

If, however, the empty molecular orbital survives transit through the Fermi Level, as happens when image charge interactions are strong at distances where the molecular electronic orbitals do not yet overlap with those of the metal surface, or when symmetry selection rules may prevent electron transfer to orbitals near the Fermi level, electron transfer may not happen until the molecule-localized hole is below the Fermi Level, where an electron may be isoenergetically transferred to the molecule, leaving an electron hole behind in the surface which is below the Fermi level (metal excited electronic state). A higher-energy electron can then relax into this hole and release energy in the form of light (chemiluminescence) or a second-excited (Auger) electron. If the energy gained by the Auger electron is larger than the work function of the surface, the electron can be emitted into vacuum and detected.

For vibrationally excited molecules, this one-dimensional view is no longer satisfactory for describing the molecule-surface interactions. In particular, the molecule's ability to bind an electron may be strongly dependent on the molecular geometry, or in the case of NO the N-O bond length. Consider specifically the vertical electron binding energy (VEBE), which is the energy difference between the neutral and anionic PESs for a molecule fixed at a specific geometry. For NO, the VEBE can be constructed as in Fig. 8. Briefly, the VEBE is found by comparing the molecular potentials for isolated neutral and anionic NO. As anion formation involves addition of an electron to an antibonding orbital, the bond length, bond strength, and harmonic frequency of the anion are all reduced compared to the neutral. This shift of the potential leads to a strong dependence of the VEBE on bond distance, spanning −200 kJ/mol at 0.8 Å—the inner turning point for NO ($\mathbf{v}''=18$)—to +200 kJ/mol at 1.6 Å—the outer turning point for NO ($\mathbf{v}''=18$).[39] Here, the neutral potential energy is about 2.1 eV *higher* in energy than that of the anion. As the work function of the surfaces used in this work is lower than 1.6 eV, it is energetically favorable to attach an electron to the molecule when it is stretched, even when the molecule is asymptotically removed from the surface.

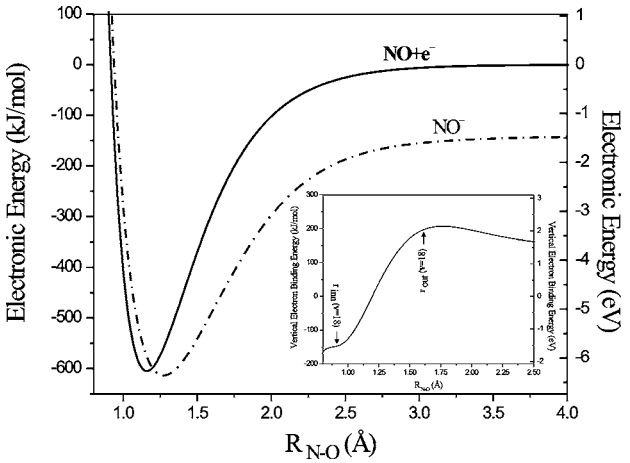

FIG. 8. Vertical electron binding energy. *Ab initio* calculations of NO (solid line) and NO^- (dashed line) to demonstrate the energetics of electron transfer. These potential-energy surfaces (PESs) are constructed as discussed in Huang *et al.* (Ref. 8). The figure inset is the vertical electron binding energy, defined as the energy difference between the neutral and anionic PESs, see text. Also shown are the inner (down arrow) and outer (upward arrow) turning points for the wave function of NO with 18 quanta of vibration.

Combining the just described characteristics of motion along the vibrational coordinate with the one-dimensional model presented at the beginning of this discussion, one can construct pictures like those shown in Figs. 9 and 10. The dashed lines in Fig. 9 illustrate the effect of the z-dependent image charge interaction for two limiting cases where the NO bond length is frozen at two bond lengths. The solid lines indicate a modeled z dependence for the neutral NO which allows it to physisorb weakly to the surface independent of it's bond length. Panel (A) shows the potential energy as a function of distance to the surface for NO fixed at its equilibrium bond length ($R=1.15$ Å). Panel (B) shows similar interactions for ($R=1.6$ Å). At infinite distance from the surface, the anionic potential (dashed line) is offset from the neutral (solid line) by the difference of the surface work function (1.6 eV) and the VEBE for this bond length. Note that at infinite separation and $R=1.15$ Å, the anion is higher in energy than the neutral, analogous with the O_2(NO $\mathbf{v}''=0$) affinity levels seen in Ref. 40 such that electron transfer is not expected.

The situation is quite different for the stretched mol-

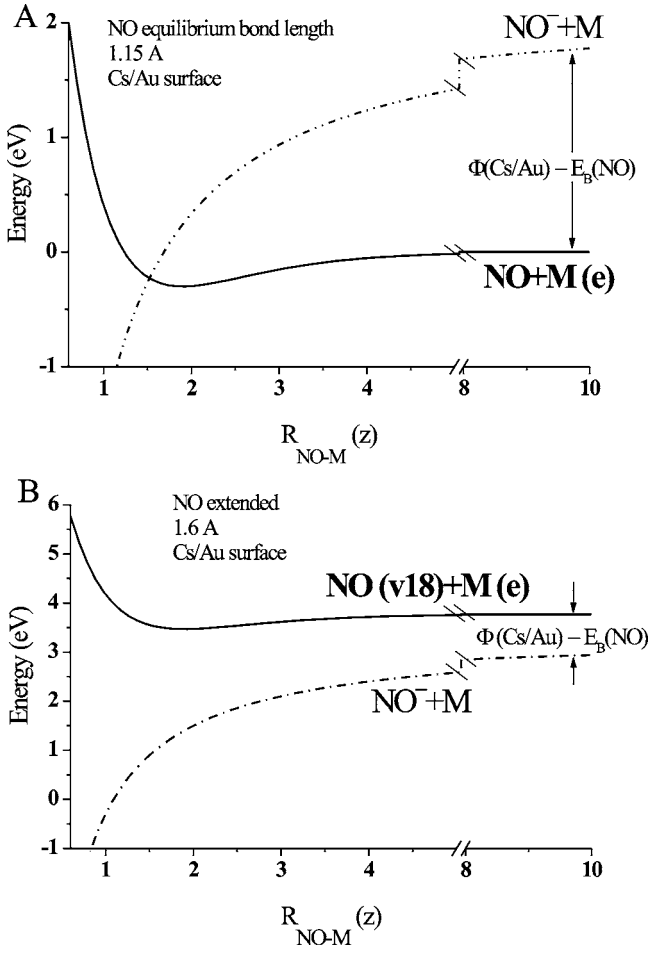

FIG. 9. Neutral and anionic potential-energy surfaces for vibrationally frozen molecules. The diagram of the approach of the NO molecule on a low work-function Cs/Au surface. The figure is based on Newn's electronic mediated interactions of NO with the metal (M) as in Ref. 12. Both panels show the NO molecule "frozen" at two bond distances. The system energy is plotted as a function of metal-molecule "center-of-mass" distance in Å. The energetic difference between the two surfaces in each panel is derived from the difference of the work function of the surface minus the vertical electron binding energy of the NO in free space. The anion curve is stabilized by the image charge as it approaches the surface. (A) The NO molecule frozen at its equilibrium bond distance of 1.15 Å. Here, the NO molecule has a negative VEBE such that the neutral PES is lower in energy than the anion PES at all but the closest molecule-surface distance. The curves eventually cross at small z. (B) The NO molecule frozen at the outer turning point for $\mathbf{v}''=18$. Here the VEBE is large and positive, meaning that the anion is lower in energy than the neutral at all bond distances. The consequence here is that at all molecule-surface distances, an electron would find it energetically favorable to reside on the molecule.

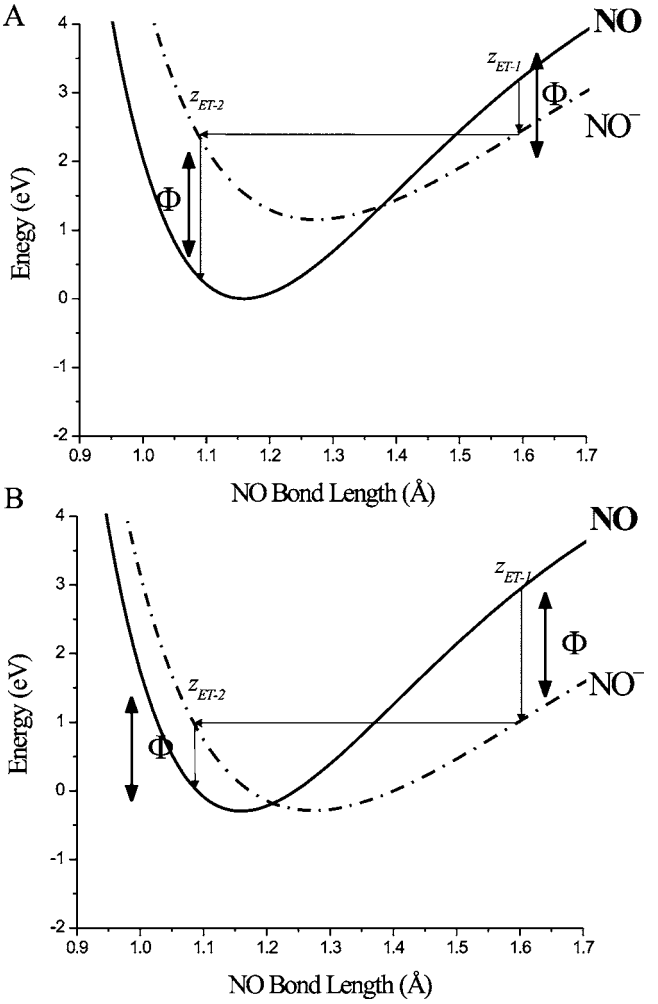

FIG. 10. Possible mechanisms for electron emission. The neutral-NO interatomic potential shows the potential energy as a function of NO separation with an electron at the Fermi level. For the NO^- potential, the electron has been transferred to the molecule. The potential curves depend strongly on the molecule-to-surface distance at which the electron transfer takes place as the NO^- potential is stabilized at shorter distances by interaction with the image charge. (A) The potential curves at "far" (10 Å) molecule-surface distance. (B) The potential curves for the case where the molecule has penetrated close (2 Å) to the surface. The magnitude of the surface work function is shown as a double-headed line.

ecule, depicted in panel (B). Here, the NO molecule is "frozen" at a bond distance of 1.6 Å, the outer turning point for $\mathbf{v}''=18$. Note that for all molecule-surface separations, the NO anion is *lower* in energy than the neutral and thus on the basis of energetic considerations it can accept an electron from below the Fermi level of the surface. Thus, the stretched NO molecule is "prepared" to allow an electron jump as soon as there is sufficient overlap of the metal and molecule electronic orbitals.

It is also useful to examine the dependence of the potential energy on vibrational coordinate (R_{N-O}) at different values of z. This is shown in Fig. 10. Here, the neutral and anionic potentials are constructed from high level electronic structure calculations of the isolated diatomics[41] as discussed by Cho.[42] At large molecule-to-surface distances (10 Å), which approximate the asymptotic limit at infinity, one obtains panel (A) of Fig. 10 where the intramolecular potential for the neutral and anionic forms of NO are shown. As z decreases, the anionic potential is shifted downward in energy by the attractive image charge interaction. In this model, we neglect the changes in the molecule-surface interaction that depend on NO bond length. The lower panel shows the neutral and anionic potentials for $z\sim 2$ Å. Also shown in Fig. 10 as downward arrows are the energetically limiting electron transfer points, the rightmost ($z_{ET\text{-}1}$) at the outer turning point for NO ($\mathbf{v}''=18$) and the leftmost at the inner turning point for the anionic PES ($z_{ET\text{-}2}$). For reference, the energetic magnitude of the work function, Φ, is shown as a bold double-headed arrow.

The previous discussion is the foundation for under-

TABLE II. Calculated magnitudes of energy transfer. The electron transfer events labeled as $z_{\text{ET-1}}$ and $z_{\text{ET-2}}$ shown in Fig. 9 are tabulated for various molecule-surface distances (z). The upper panel of the table is the energy separation between the neutral and anion at the outer turning point for the vibrationally excited molecules. The lower panel is a consequence of isoenergetic compression of the anion formed from attaching an electron from the surface, and then transferring the electron when the molecule bond distance reaches the anionic inner turning point.

	$\mathbf{v}''=18$	$\mathbf{v}''=10$	$\mathbf{v}''=9$	$\mathbf{v}''=8$	$\mathbf{v}''=7$
z (Å)	$\Delta E z_{\text{ET-1}}$(eV)	$\Delta E z_{\text{ET-1}}$(eV)	$\Delta E z_{\text{ET-1}}$(eV)	$\Delta E z_{\text{ET-1}}$(eV)	$\Delta E z_{\text{ET-1}}$(eV)
10	0.87	0.49	0.41	0.31	0.21
8	0.96	0.58	0.50	0.40	0.30
6	1.10	0.73	0.64	0.55	0.44
3	1.56	1.18	1.10	1.00	0.90
1.9	2.21	1.84	1.64	1.55	1.44
z (Å)	$\Delta E z_{\text{ET-2}}$(eV)	$\Delta E z_{\text{ET-2}}$(eV)	$\Delta E z_{\text{ET-2}}$(eV)	$\Delta E z_{\text{ET-2}}$(eV)	$\Delta E z_{\text{ET-2}}$(eV)
10	2.24	1.78	1.70	1.61	1.51
8	2.15	1.70	1.61	1.52	1.42
6	2.00	1.55	1.47	1.38	1.28
3	1.55	1.10	1.01	0.93	0.83
1.9	0.89	0.44	0.47	0.38	0.28

standing charge-transfer events when vibrationally excited molecules scatter from low work-function metal surfaces. We now present three possible mechanisms.

In evaluating any mechanism, it is imperative that it easily explains the two key experimental observations.

(1) We do not detect electron emission when the vibrational energy is lower than the work function of the surface.
(2) The magnitude of the quantum efficiency is between 1% and 3% for the highest vibrational states studied; at least two orders of magnitude larger than similar systems.[43]

Mechanism 1: Vibrationally promoted autodetachment

If the initial electron transfer event occurs at large molecule-surface distances (z), Fig. 10(a) provides a reasonable description of the situation. Here, electron transfer is most likely to occur near the outer vibrational turning point. Because the neutral-anionic energy separation at the outer turning point, $z_{\text{ET-1}}$ will be smaller than the work function of the surface even for NO ($\mathbf{v}''=18$), the energy released in this event is not expected to be sufficient to eject an electron from the surface.

As the anionic molecule compresses, the potential energy of the transferred electron increases by as much as 3 eV at the inner turning point of vibration, putting the system in an excited electronic state. If the electron is lost from the NO near the inner turning point, the electron can be ejected into vacuum, provided enough vibrational energy is converted to the translation of the electron.

According to the influential Noerskov-Newns-Lundqvist (NNL) paper,[44] it is energetically feasible for alkali metals to transfer an electron to an electrophillic molecule at molecule-surface distances as large as ~10–30 Å; the situation shown in Fig. 10(a). In order to be more specific we consider explicitly the z distance of 10 Å. Here, only 0.87 eV of energy is lost when the electron transfers to NO ($\mathbf{v}''=18$) at $z_{\text{ET-1}}$, but 2.24 eV of energy is released from the molecule by the electron transfer event at $z_{\text{ET-2}}$, easily enough to overcome the (1.3–1.6 eV) work function and carry the electron away from the surface. So, the vibrational autodetachment mechanism can explain, at least on energetic grounds, the vibrational promotion of electron emission for NO ($\mathbf{v}''=18$).

A similar analysis for various initial vibrational states and molecule-surface distances can be carried out and is presented in Table II. Here, the energy released when the electron transfers *to* the neutral NO molecule (top of Table II) and *from* the NO anion (bottom of Table II) is shown. This will help to identify the trends for energy transfer as the molecule approaches the surface in various vibrational states and reveal possible explanations for the threshold behavior.

The reader will forebear us some degree of imprecision in this discussion as the work function of the surface (1.3–1.6 eV) is, unfortunately, not well determined in this work. Despite this, we note what appears to be a meaningful feature of the threshold behavior, namely, the vibrational energy at threshold slightly overshoots the work function. That is, the first vibrational state that clearly produces electron emission is $\mathbf{v}''=9$, with 2.11 eV vibrational energy, possibly as far as 0.8 eV above the work function. It is noteworthy that the vibrational autodetachment mechanism appears to predict such an overshoot. Again assuming that the electron transfer happens at $z\sim10$ Å, inspection of Table II reveals that NO ($\mathbf{v}''=7$) and NO ($\mathbf{v}''=8$) release 1.51 and 1.61 eV at $z_{\text{ET-2}}$, respectively. In the event that the surface work function were as large as 1.6 eV, this would be consistent with the observation of $\mathbf{v}''=9$ as the first electron producing vibrational state.

This autodetachment mechanism appears to be consistent with the observed (~2%) quantum yields simply because this mechanism requires a single electron transferring to and from the molecule. Assuming that the initial electron transfer is facile, we might imagine that the majority of the vibrational autodetachment events happen at compressed

N–O bond lengths larger than the inner turning point, leading to excited electrons with energies less than the work function. Thus, only that small fraction of the quantum probability flux still present as the NO anion when the inner turning point is reached may produce electrons with enough energy to overcome the work function. Of course, rigorous theoretical work in the future will be required to verify this line of reasoning.

There is precedence for this mechanism to be viable elsewhere in the literature. Böttcher[45] has investigated exoemission during the scattering of vibrationally excited N_2O ($\mathbf{v}_2=1$) on a 250 K Cs/Ru(0001) surface. Here, they found the exoemission for hot N_2O was 20 times larger than that for $\mathbf{v}=0$. N_2O is known to easily dissociate into N_2+O^- after electron attachment (harpooning),[46] the probability of which increases as the bending mode is excited. Böttcher postulated that harpooning was the primary mechanism for exoemission when N_2O oxidizes the surface.[45] By measuring the electron emission and N_2 abstraction from the Cs surface, they were able to indirectly determine the likelihood for the formation of a bond between the O^- and Cs atoms during the dissociation process. They compared the amount of N_2 from hot (containing vibrationally excited) and cold (vibrational ground state) N_2O beams and found that the vibrationally excited molecules enhanced N_2 abstraction by a factor of 3. Harpooning mediated dissociation was clearly not sufficient to explain the factor of 20 increase in exoemission. The mechanism of autodetachment,

$$N_2O^{-*} + M \rightarrow N_2O + e + M, \tag{6}$$

similar to what we describe here, was one of the three nondissociative mechanism invoked to explain this discrepancy.

Mechanism 2: Electron emission via Auger deexcitation

A major issue in the discussion of these possible mechanisms concerns our lack of knowledge about the typical values of z, where the first electron transfer, $z_{\text{ET-1}}$, takes place. As just described, if $z_{\text{ET-1}}$ is rather large, vibrational autodetachment can be an important mechanism for the ejection of electrons. On the other hand, if $z_{\text{ET-1}}$ were to be as small as 1–2 Å, another mechanism of vibrationally promoted electron emission becomes possible. Here the energetics of Fig. 10(b) are relevant. If the tunneling from surface to molecule cannot take place without these intimate collisions, the affinity level on the molecule represents a high-energy "hole," with perhaps as much as 3 eV of excitation. An electron that isoenergetically transfers from ~3 eV below the Fermi level to this molecule-centered hole, will create a high-energy hole in the metal, that is subject to filling through Auger relaxation, resulting in secondary electron emission into vacuum. Subsequent bond compression of the anion again raises the potential energy of the NO-bound electron possibly above the Fermi level where it might retransfer to the metal surface.

We now consider what predictions a model based on the Auger mechanism would make concerning the NO vibrational state dependence. Again, referring to Table II is quite helpful. For the Auger mechanism it is the energy, $\Delta E z_{\text{ET-1}}$, that can lead to electron ejection, which strongly depends on z and $\mathbf{v}$. Referring to Table II, a threshold consistent with Fig. 7 (occurring at $\mathbf{v}''=9$) for electron emission via the Auger mechanism is predicted for molecule-surface distances *of about* 1.9 Å; here we must assume that the surface work function is 1.6 eV. Thus, the affinity level must survive passage below the Fermi level up to a rather small distance to the surface.

The question now becomes "is this likely?" To answer this question, it is perhaps helpful to compare the relative time scales of the two degrees of freedom (z and $R_{\text{N-O}}$). According to Herzberg,[31] classically, the vibrational frequency (f_{osc}) of an anharmonic oscillator in state $\mathbf{v}$ follows the expression

$$f_{\text{osc}}(\mathbf{v}) = c \bullet \Delta G_{\mathbf{v}}, \tag{7}$$

where $\Delta G_{\mathbf{v}}$ is the energy of the vibrational level using constants presented by Amiot[47] for NO in vibrational states up to $\mathbf{v}''=22$. From this classical oscillator frequency, NO ($\mathbf{v}''=18$) has a period of vibration of 24 fs. For comparison, NO ($\mathbf{v}''=9$) has a period of 20 fs. The approximate time scale for NO with 29 meV of translational energy to approach the surface from 8 Å (where autodetachment is suggested to occur) to 2 Å (where Auger emission is expected) is on the order of 1.3 ps, neglecting any acceleration the neutral molecule might experience. Thus, NO undergoes more that 50 vibrational periods as it approaches the surface between 8 and 2 Å.

From the chemical hole diving model developed by Greber,[35] it is possible to estimate the hole survival probability in a similar system, $P_h(t)$, for the unoccupied molecular orbital as it approaches the surface. The survival probability is described as

$$P_h(t) = \exp[-t^3/(3t_e^2\tau_e)], \tag{8}$$

where t_e is the diving time to the maximum binding energy (ε_A) for the unoccupied orbital, and τ_e is the lifetime of a hole state at ε_A. τ_e can be calculated from the width of the energy distribution of electron emission, which was not measured here. We can approximate the lifetime of a hole state at ε_A by looking at a similar system of O_2 on Cs. Greber estimated τ_e for O_2 on Cs,[37] leading to a reaction time of ~100 fs before the hole filling. The likelihood of the orbital remaining unoccupied over the 1.3 ps transit time thus appears small. On the other hand, our level of certainty about the basic nature of electronically nonadiabatic phenomena in molecule-metal interactions is sufficiently meager, that we should hesitate to discard this possibility out of hand.

It is furthermore not clear that the Auger mechanism is consistent with the high quantum efficiencies seen in this work. A traditional Auger process requires multiple charge-transfer events, where the electron first hops to the molecule, followed by an energy release that interacts with a surface electron and gives it enough energy in a perpendicular escape vector to be ejected from the surface. There is also a probability that the surface electron is scattered off neighboring electrons, imparting some kinetic energy back into the surface electronic structure. The combination of these sequential events may result in a relatively rare emission event. It is perhaps for this reason that previous explanations of

exoemission that exhibited a probability for exoelectron emission on the order of 10^{-4}–10^{-8} were consistent with an Auger-type mechanism. These values are, however, at least two orders of magnitude smaller than those reported here again leaning the impartial reader to more strongly consider the vibrational autodetachment mechanism as a likely candidate.

Mechanism 3: Surface-induced molecular dissociation

The final mechanism addressed here that might possibly explain our results involves NO molecules dissociating into atomic constituents on the surface. Recent experiments have observed NO dissociation on cold (190 K) Cs/Ru metal surfaces prior to electron emission.[40] In that work, an oxidized surface (from N+O) was required for further NO molecules to penetrate near to the surface for Auger emission to occur. There is evidence elsewhere in the literature[48] that NO does not dissociatively adsorb on Cs surfaces warmer than 220 K, and because our experiments were carried out at room temperature, we believe that dissociation is not the explanation for our observed electron emission.

This is further emphasized by the observation that we see no measurable signal from a molecular beam of NO ($\mathbf{v}''=0$). Of course, it could be argued that large amplitude vibrational motion could aid in the dissociation of molecules on surfaces by helping surmount some barrier in the reactive potential-energy surface. Why this barrier would coincidentally be close in height to the value of the surface work function remains a difficult point to reconcile within this context.

There are other significant differences between this and the work of Böttcher *et al.* on NO.[40] First, White *et al.*[32] recently reported NO vibrationally promoted electron emission as a function of O_2 exposure to a Cs/Au surface. Unlike the observations of Böttcher *et al.*, electron emission began immediately upon introduction of the vibrationally excited NO molecules and qualitatively followed the expected change in work function as the surface was oxidized from concurrent introduction of O_2. As was argued by White *et al.*, there was no requirement for the surface to be preoxidized by molecular dissociation before electron emission occurred; a stringent requirement in the work of Böttcher *et al.*. In order to eliminate (or support) the dissociation mechanism, experiments that probe postscattering must be carried out. These include probing the scattered product, searching for NO, N_2O, and possibly N_2 which is not known to reside on Cs surfaces, and to investigate the surface for adsorbed oxygen atoms.

CONCLUSION

Electron emission as a function of vibrational energy for vibrationally excited NO molecules striking a low work-function Cs/Au surface has a threshold at a vibrational energy slightly larger then the work function of the surface. The quantum yield is large ($>10^{-2}$) for vibrational energies well above the threshold. The fact that the vibrational energy threshold is slightly larger than the work function appears to be an important clue to a deeper understanding of these phenomena. Three model mechanisms were presented and discussed. A mechanism of vibrationally promoted autodetachment appears to be the most likely candidate to explain these observations, a mechanism previously suggested in connection with measurements of vibrational relaxation of highly vibrationally excited NO molecules.[16]

Future experiments will promise to bring greater clarity to understanding the primary mechanism for electron emission induced by vibrationally excited molecules. Monitoring the survival probability of NO in various vibrational states scattering from the surface will help quantify the amount of energy lost during charge transfer and will conclusively rule out (or support) molecular dissociation. An electron energy analyzer will soon be built to measure the energy distribution of the electrons emitted during the experiment.

Regardless of the mechanism, the work presented here indicates that violations of the Born-Oppenheimer approximation may play a role that cannot be safely ignored during gas-surface interactions; especially when the molecules are highly vibrationally excited. The ramifications of these findings suggest a reanalysis of the methods used to model surface chemical reactions which, in turn, may aid in the development of newer, better catalytic systems.

ACKNOWLEDGMENTS

The work was supported by a grant from the National Science Foundation (CHE0135581) and a grant from the Department of Energy Office of Basic Energy Sciences (DE-FG02-03ER15441). The UCSB group would also like to acknowledge Terry Hart and the UCSB machine shop for all the work done to construct a functioning machine.

[1] *Environmental Catalysis*, edited by J. N. Armor, Denver, CO, 28 March–2 April, 1993.
[2] See, for example, S. A. Harich, D. X. Dai, C. C. Wang, X. M. Yang, S. D. Chao, and R. T. Skodje, Nature (London) **419**, 281 (2002).
[3] M. Born and E. Oppenheimer, Ann. Phys. **84**, 457 (1927).
[4] M. Head-Gordon and J. C. Tully, J. Chem. Phys. **103**, 10137 (1995).
[5] A. M. Wodtke, J. C. Tully, and D. J. Auerbach, Int. Rev. Phys. Chem. **23**, 513 (2004).
[6] H. S. W. Massey, Rep. Prog. Phys. **12**, 248 (1949).
[7] C. J. Zhang, P. Hu, and A. Alavi, J. Chem. Phys. **112**, 10564 (2000).
[8] C. Bungaro, C. Noguera, P. Ballone, and W. Kress, Phys. Rev. Lett. **79**, 4433 (1997).
[9] G. J. Kroes, Prog. Surf. Sci. **60**, 1 (1999).
[10] C. T. Rettner, F. Fabre, J. Kimman, and D. J. Auerbach, Phys. Rev. Lett. **55**, 1904 (1985).
[11] J. W. Gadzuk and S. Holloway, Phys. Rev. B **33**, 4298 (1986).
[12] D. M. Newns, Surf. Sci. **171**, 600 (1986).
[13] G. A. Gates and S. Holloway, Surf. Sci. **309**, 132 (1994).
[14] A. Gross and W. Brenig, Chem. Phys. **177**, 497 (1993).
[15] Y. Huang, A. M. Wodtke, H. Hou, C. T. Rettner, and D. J. Auerbach, Phys. Rev. Lett. **84**, 2985 (2000).
[16] Y. H. Huang, C. T. Rettner, D. J. Auerbach, and A. M. Wodtke, Science **290**, 111 (2000).
[17] A. M. Wodtke, Y. H. Huang, and D. J. Auerbach, J. Chem. Phys. **118**, 8033 (2003).
[18] S. M. Li and H. Guo, J. Chem. Phys. **117**, 4499 (2002).
[19] J. D. White, J. Chen, D. Matsiev, D. J. Auerbach, and A. M. Wodtke, Nature (London) **433**, 503 (2005).
[20] M. Skottkeklein, A. Böttcher, R. Imbeck, S. Kennou, A. Morgante, and G. Ertl, Thin Solid Films **203**, 131 (1991).
[21] C. Kittrell, E. Abramson, J. L. Kinsey, S. A. McDonald, D. E. Reisner, R. W. Field, and D. H. Katayama, J. Chem. Phys. **75**, 2056 (1981); M.

Silva, R. Jongma, R. W. Field, and A. M. Wodtke, Annu. Rev. Phys. Chem. **52**, 811 (2001).
[22] Two laser beams, collinearly overlapped with a 20 ns relative time delay, interacted with the molecular beam 9 cm from the nozzle and 6 cm after the skimmer to effectuate SEP (P-D in Fig. 1). SEP in NO transfers population from $v''=0$ into the excited final vibrational state in a two-step process. The first or "pump" laser (P) excites the molecule to a low vibrational level of a higher electronic state, v', and the second or "dump" laser (D) stimulates emission back to a target high vibrational level of a ground electronic state, v''. Laser-induced fluorescence (LIF) was used to monitor the pump step and fluorescence depletion was used to quantify the fractional deexcitation achieved through stimulated emission in the dump step. Both processes were measured using a photomultiplier (PMT1-Hammamatsu R212UH).
[23] For an example of the technique, see M. Fuchs and J. P. Toennies, J. Chem. Phys. **85**, 7062 (1986).
[24] J. Chen, D. Matsiev, J. D. White, M. Murphy, and A. M. Wodtke, Chem. Phys. **301**, 161 (2004).
[25] The gain of the PMT could be measured by examining peak heights of single-photon events on the oscilloscope. The collection efficiency of the imaging system was calculated from its geometry, leading to a value of 15%. In short, we make use of a one-to-one imaging system with two lenses (CVI Lasers Model. BICX-50.8-48.9-UV fused silica biconvex spherical lenses) with an estimated reflective loss of 5% per lens. The assembly also contains a concave spherical reflector (Precision Applied Products Model PAP-CSR0300) coated for 80%–90% reflectivity over the range of 200–400 nm.
[26] Our crystal at one time was Au(111) but we strongly suspect that surface has lost its ordered structure and may have been twinned through use.
[27] C. S. Wang, J. Appl. Phys. **48**, 1477 (1977).
[28] J. L. Wiza, Nucl. Instrum. Methods **162**, 587 (1979).
[29] Two sets of MCP's with 18-mm-diam active area and 40-mm-diam active area were used in two sets of experiments in order to gauge the electron collection efficiency of our system. To insure that all of the negative particles were collected, a 2–3 G magnetic field was used to steer these particles onto the detector in order to generate the largest signal. Using the 18 mm MCP's, the magnetic steering was essential to obtain reasonable collection efficiency. With the 40 mm MCP detector, the magnetic steering was less critical; 60% of the emitted particles could be collected without magnetic steering and the signals were two to three times larger than for the 18 mm detector. The strong dependence on detector size and weak magnetic fields is the evidence that the detected particles are electrons. The results reported in this work were obtained with the 40 mm MCP detector.
[30] Several experimental factors were necessary when determining N_{18}. The spatial overlap of the probe laser with the pulsed molecular beam means only a small fraction of the vibrationally excited molecules can be induced to fluoresce by the probe laser. This fraction was easily calculable from the geometry of our system. The fluorescence intensity was recorded on an averaging oscilloscope as a voltage across a 50 Ω resistor. Integration of this signal yielded the total charge produced from the photomultiplier which, when considered in the context of the wavelength-dependent gain of the PMT and collection efficiency of the fluorescence imaging system, gave the number of molecules contributing to the fluorescence.
[31] G. Herzberg, *Molecular Spectra and Molecular Structure*, Spectra of Diatomic Molecules Vol. I 2nd ed. Twelfth Printing. (Van Nostrand, Princeton, 1967).
[32] J. D. White, J. Chen, D. Matsiev, D. J. Auerbach, and A. M. Wodtke, J. Vac. Sci. Technol. A **23**, 1085 (2005).
[33] J. Luque and D. R. Crosley, J. Chem. Phys. **111**, 7405 (1999).
[34] M. Drabbels and A. M. Wodtke, J. Chem. Phys. **106**, 3024 (1997).
[35] T. Greber, Chem. Phys. Lett. **222**, 292 (1994).
[36] A. Böttcher, R. Grobecker, R. Imbeck, A. Morgante, and G. Ertl, J. Chem. Phys. **95**, 3756 (1991).
[37] T. Greber, Surf. Sci. Rep. **28**, 1 (1997).
[38] J. W. Gadzuk and J. K. Noerskov, J. Chem. Phys. **81**, 2828 (1984).
[39] The wave function is calculated using the potentials constructed by the RKR method with a program written in MATHEMATICA similar to that described by P. Senn, Comput. Chem. (Oxford) 19, 437 (1995). The constants for the NO molecule are from G. Herzberg. *Molecular Spectra and Molecular Structure*, Spectra of Diatomic Molecules Vol. I, 2nd ed. (Van Nostrand, Princeton, 1967). The probability is calculated from squaring the wave function found by fitting the energies for the NO molecule to the NO RKR potential and integrating in the between 1.61 and 1.73 Å. From this, it is found that NO spends 30% of its time at the outer turning point.
[40] A. Böttcher, R. Grobecker, T. Greber, and G. Ertl, Chem. Phys. Lett. **208**, 404 (1993).
[41] M. C. McCarthy, J. W. R. Allington, and K. S. Griffith, Chem. Phys. Lett. **289**, 156 (1998).
[42] S.-W. Cho, Journal of the Korean Chemical Society **46**, 14 (2002).
[43] H. Brenten, H. Mueller, W. Maus-Friedrichs, S. Dieckhoff, and V. Kempter, Surf. Sci. **262**, 151 (1992).
[44] J. K. Noerskov, D. M. Newns, and B. I. Lundqvist, Surf. Sci. **80**, 179 (1979).
[45] A. Böttcher, Langmuir **17**, 3348 (2001).
[46] P. J. Chantry, J. Chem. Phys. **51**, 3369 (1969).
[47] C. Amiot, J. Mol. Spectrosc. **94**, 150 (1982).
[48] A. F. Carley, M. W. Roberts, and A. K. Santra, Surf. Sci. **516**, L523 (2002).